Dissipationless collapse of a set of N massive particles

Fabrice Roy[(1)][⋆] and Jérôme Perez[(1,2)][†]

[(1)]*École Nationale Supérieure de Techniques Avancées, Unité de Mathématiques Appliquées, 32 Bd Victor, 75015 Paris, France*

[(2)]*Laboratoire de l'Univers et de ses THéories, Observatoire de Paris-Meudon, 5 place Jules Janssen, 92350 Meudon, France*

23 September 2003

ABSTRACT

The formation of self-gravitating systems is studied by simulating the collapse of a set of N particles which are generated from several distribution functions. We first establish that the results of such simulations depend on N for small values of N. We complete a previous work by Aguilar & Merritt concerning the morphological segregation between spherical and elliptical equilibria. We find and interpret two new segregations: one concerns the equilibrium core size and the other the equilibrium temperature. All these features are used to explain some of the global properties of self-gravitating objects: origin of globular clusters and central black hole or shape of elliptical galaxies.

Key words: methods: numerical, N-Body simulations – galaxies: formation – globular clusters: general.

1 INTRODUCTION

It is intuitive that the gravitational collapse of a set of N masses is directly related to the formation of astrophysical structures like globular clusters or elliptical galaxies (the presence of gas may complicate the pure gravitational N-body problem for spiral galaxies). From an analytical point of view, this problem is very difficult. When N is much larger than 2, direct approach is intractable, and since Poincaré results of non analyticity, exact solutions may be unobtainable. In the context of statistical physics, the situation is more favorable and, in

---

⋆ roy@ensta.fr

† perez@ensta.fr

a dissipationless approximation[1], leads to the Collisionless Boltzmann Equation (hereafter denoted by CBE)

$$\frac{\partial f}{\partial t} + \mathbf{p}.\frac{\partial f}{\partial \mathbf{r}} + m\frac{\partial \psi}{\partial \mathbf{r}}.\frac{\partial f}{\partial \mathbf{p}} = 0 \tag{1}$$

where $f = f(\mathbf{r}, \mathbf{p}, t)$ and $\psi = \psi(\mathbf{r}, t)$ are respectively the distribution function of the system with respect to the canonically conjugated $(\mathbf{r}, \mathbf{p})$ phase space variables and the mean field gravitational potential. As noted initially by Hénon (1960), this formalism holds for such systems if and only if we consider N identical point masses equal to m. This problem splits naturally into two related parts: the time dependent regime and the stationary state. We can reasonably think that these two problems are not completely understood. The transient time dependent regime was investigated mainly considering self-similar solutions (Lynden-Bell & Eggleton (1980), Henriksen & Widrow (1995), Blottiau et al. (1988) and Lancellotti & Kiessling (2001)). These studies conclude that power law solutions can exist for the spatial dependence of the gravitational potential (with various powers). Nevertheless, there is no study which indicates clearly that the time dependence of the solutions disappears in a few dynamical times, giving a well defined equilibrium-like state. On the other hand, applying Jeans theorem (e.g. Binney & Tremaine (1987) hereafter BT87, p. 220), it is quite easy to find a stationary solution. For example, every positive and integrable function of the mean field energy per mass unit E is a potential equilibrium distribution function for a spherical isotropic system. Several approaches are possible to choose the equilibrium distribution function. Thermodynamics (Violent Relaxation paradigm: Lynden-Bell (1967), Chavanis (2002), Nakamura (2000)) indicate that isothermal spheres or polytropic systems are good candidates. Stability analyses can be split into two categories. In the CBE context (see Perez & Aly (1998) for a review), it is well known that spherical systems (with decreasing spatial density) are generally stable except in the case where a large radial anisotropy is present in the velocity space. This is the Radial Orbit Instability, hereafter denoted by ROI (see Perez & Aly (1998), and Perez et al. (1998) for a detailed analytic and numeric study of these phenomena) which leads to a bar-like equilibrium state in a few dynamical times. In the context of thermodynamics of self-gravitating systems, in a pioneering work

---

[1] The dissipationless hypothesis is widely accepted in the context of gravitational N-body problem because the ratio of the two-body relaxation time over the dynamical time is of the order of N. For a system composed of more than $\sim 10^4$ massive particles a study during a few hundreds dynamical times can really be considered as dissipationless, the unique source of dissipation being two-body encounters.

by Antonov (1962), it was shown that an important density contrast leads to the collapse of the core of system (see Chavanis (2003) for details).

In all these studies there is no definitive conclusion, and the choice of the equilibrium distribution remains unclear. Introducing observations and taking into account analytical constraints, several models are possible: chronologically, we can cite (see for example BT87, p. 223-239) the Plummer model (or other polytropic models), de Vaucouleurs $r^{1/4}$ law, King and isochrone Hénon model or more recently the very simple but interesting Hernquist model (Hernquist (1990)) for spherical isotropic systems. In the anisotropic case, Ossipkov-Merritt or generalized polytropes can be considered. Finally for non spherical systems, there also exists some models reviewed in BT87 (p. 245-266). Considering this wide variety of possibilities, one can try to make accurate numerical simulations to clarify the situation. Surprisingly, such a program has not been completely carried on. In a pioneering work, van Albada (1982) remarked that the dissipationless collapse of a clumpy cloud of N equal masses could lead to a final stationary state that is quite similar to elliptical galaxies. This kind of study was reconsidered in an important work by Aguilar & Merritt (1990), with more details and a crucial remark concerning the correlation between the final shape (spherical or oblate) and the virial ratio of the initial state. These authors explain this feature invoking ROI. Some more recent studies (Cannizzo & Hollister (1992), Boily et al. (1999) and Theis & Spurzem (1999)) concentrate on some particularities of the preceding works. Finally, two works (Dantas et al. (2002) and Carpintero & Muzzio (1995)) develop new ideas considering the influence of the Hubble flow on the collapse. However, the problem is only partially depicted.

The aim of this paper is to analyse the dissipationless collapse of a large set of N Body systems with a very wide variety of 'realistic' initial conditions. As we will see, the small number of particles involved, the numerical technique or the specificity of the previous works did not allow their authors to reach a sufficiently precise conclusion. The layout of this paper is as follows. In section 2 we describe in detail the numerical procedures used in our experiments. Section 3 describes the results we have obtained. These results are then interpreted in section 4, where some conclusions and perspectives are also proposed.

2 NUMERICAL PROCEDURES

2.1 Dynamics

The Treecode used to perform our simulations is a modified version of the Barnes & Hut (1986) Treecode, parallelised by D. Pfenniger using the MPI library. We implemented some computations of observables and adapted the code to suit our specific problems. The main features of this code are a hierarchical $O(N \log(N))$ algorithm for the gravitational force calculation and a leap-frog algorithm for the time integration. We introduced an adaptative time step, based on a very simple physical consideration. The time step is equal to a fraction n_{ts} of the instantaneous dynamical time T_d ([2]) , i.e. $\Delta t = T_d/n_{ts}$. The simulations were run on a Beowulf cluster (25 dual CPU processors whose speed ranges from 400MHz to 1GHz).

2.2 Initial Conditions

The initial virial ratio is an important parameter in our simulations. The following method was adopted to set the virial ratio to the value $V_{initial}$. Positions $\mathbf{r}_i$ and velocities $\mathbf{v}_i$ are generated. We can then compute

$$V_p = \frac{2K}{U} \tag{2}$$

where

$$K = \sum_{i=1}^{N} \frac{1}{2} m_i \mathbf{v}_i^2 \tag{3}$$

and

$$U = -\frac{G}{2} \sum_{i \neq j}^{N} \frac{m_i m_j}{\left(max((\mathbf{r}_i - \mathbf{r}_j)^2, \epsilon^2)\right)^{1/2}} \quad . \tag{4}$$

In this relation ϵ is a softening parameter whose value is discussed in section 2.3.2. As the potential energy depends only on the positions, we obtain a system with a virial ratio equal to $V_{initial}$ just by multiplying all the particle velocities by the factor $(V_{initial}/V_p)^{1/2}$. For convenience we define

---

[2] The fraction n_{ts} is adapted to the virial parameter η and ranges roughly from $n_{ts} = 300$ when $\eta = 90$ to $n_{ts} = 5000$ when $\eta = 08$. The dynamical time we used is given by

$$T_d = \frac{\sum\limits_{i=1}^{N} \sqrt{x_i^2 + y_i^2 + z_i^2}}{\sum\limits_{i=1}^{N} \sqrt{vx_i^2 + vy_i^2 + vz_i^2}}$$

$$\eta = |V_{initial}| \times 10^2 \tag{5}$$

2.2.1 Homogeneous density distribution (H_η)

As we study large N-body systems, we can produce a homogeneous density by generating positions randomly. These systems are also isotropic. We produce the isotropic velocity distribution by generating velocities randomly.

2.2.2 Clumpy density distribution (C_η^n)

A type of inhomogeneous systems is made of systems with a clumpy density distribution. We first generate n small homogeneous spherical systems with radius R_g. Centers of these subsystems are uniformly distributed in the system. The empty space is then filled using a homogeneous density distribution. In the initial state, each clump contains about 1% of the total mass of the system and have a radius which represents 5% of the initial radius of the whole system. These systems are isotropic.

2.2.3 Power law $r^{-\alpha}$ density distribution (P_η^α)

We first generate the φ and z cylindrical coordinates using two uniform random numbers u_1 and u_2:

$$(z, \varphi) = (2u_1 - 1, 2\pi u_2) \quad . \tag{6}$$

Using the inverse transformation method, if

$$r = RF^{-1}(u) \quad \text{with} \quad F(r) = \frac{1}{S} \int_\iota^r x^{2-\alpha} dx \tag{7}$$

where R is the radius of the system, u is a uniform random number, $\iota \ll 1$ and

$$S = \int_0^1 x^{2-\alpha} dx \quad , \tag{8}$$

then the probability density of r is proportional to $r^{2-\alpha}$, and the mass density ρ is proportional to $r^{-\alpha}$. Finally, one gets

$$\mathbf{r} = \begin{bmatrix} r\sqrt{1-z^2} \cos\varphi \\ r\sqrt{1-z^2} \sin\varphi \\ rz \end{bmatrix} \tag{9}$$

These systems are isotropic.

2.2.4   *Gaussian velocity distribution(G_η^σ)*

Most of the systems we use have a uniform velocity distribution. But we have also performed simulations with systems presenting a gaussian initial velocity distribution. These systems are isotropic, but the x-, y- and z-components of the velocity are generated following a gaussian distribution. Using a standard method we generate two uniform random numbers u_1 and u_2, and set

$$v_i = \sqrt{-2\sigma^2 \ln u_1} \cos(2\pi\sigma^2 u_2) \qquad i = x, y, z \tag{10}$$

where σ is the gaussian standard deviation.

2.2.5   *Global rotation (R_η^f)*

Some of our initial systems are homogeneous systems with a global rotation around the Z-axis. The method we choose to generate such initial conditions is the following. We create a homogeneous and isotropic system (an H-type system). We then compute the average velocity of the particles.

$$\bar{v} = \frac{1}{N} \sum_{i=1}^{N} \|\mathbf{v}_i\| \tag{11}$$

We project the velocities on a spherical referential, and add a fraction of $\bar{v}$ to v_ϕ with regard to the position of the particle. We set

$$v_{i,\phi} = v_{i,\phi} + f\frac{\rho_i \bar{v}}{R} \tag{12}$$

where f is a parameter of the initial condition, ρ_i is the distance from the particle to the Z-axis and R the radius of the system. The amount of rotation induced by this method can be evaluated through the ratio:

$$\mu = K_{rot}/K, \tag{13}$$

where K is the total kinetic energy defined above, whereas K_{rot} is the rotation kinetic energy defined by Navarro & White (1993):

$$K_{rot} = \frac{1}{2} \sum_{i=1}^{N} m_i \frac{(\mathbf{J}_i \cdot \hat{\mathbf{J}}_{tot})^2}{[\mathbf{r}_i^2 - (\mathbf{r}_i \cdot \hat{\mathbf{J}}_{tot})^2]} \tag{14}$$

Above, $\mathbf{J}_i$ is the specific angular momentum of particle i, $\hat{\mathbf{J}}_{tot}$ is a unit vector in the direction of the total angular momentum of the system. In order to exclude counter-rotating particles, the sum in equation (14) is actually carried out only over those particles which verify the condition $(\mathbf{J}_i \cdot \hat{\mathbf{J}}_{tot}) > 0$.

2.2.6 Power-law initial mass function(M_η^k)

Almost all the simulations we made assume particles with equal masses. However, we have created some initial systems with a power-law mass function, like

$$n(M) = \alpha M^\beta \tag{15}$$

The number of particles whose mass is $M \leqslant m \leqslant M + dM$ is $n(M)dM$. In some models, the value of α and β depends on the range of mass that is considered. We have used several types of mass functions, among them the initial mass function given by Kroupa (2001) ($k = I$), the one given by Salpeter (1955) ($k = II$) and an M^{-1} mass function ($k = III$). In order to generate masses following these functions, we first calculate α_k to produce a continuous function. We then can calculate the number of particles whose mass is between M and $M + dM$. We generate $n(M)$ masses

$$m_i = M + udM \qquad\qquad 1 \leqslant i \leqslant n(M) \tag{16}$$

where $0 \leqslant u \leqslant 1$ is a uniform random number. In the initial state, these systems have a homogeneous number density, a quasi homogeneous mass density and they are isotropic.

2.2.7 Nomenclature

We indicate below the whole set of our non rotating initial conditions.

- Homogeneous H_η models: H_{88}, H_{79}, H_{60}, H_{50}, H_{40}, H_{30}, H_{20}, H_{15} and H_{10}
- Clumpy C_η^n models: C_{67}^{20}, C_{65}^{20}, C_{61}^{20}, C_{48}^{20}, C_{39}^{20}, C_{29}^{20}, C_{14}^{20}, C_{10}^{20}, C_{07}^{20} and C_{10}^{03}
- Power Law P_η^α models: $P_{50}^{2.0}$, $P_{09}^{2.0}$, $P_{50}^{1.0}$, $P_{50}^{0.5}$, $P_{10}^{1.0}$, $P_{08}^{1.5}$ and $P_{40}^{1.5}$
- Gaussian velocity profiles G_η^σ models: G_{50}^1, G_{50}^2, G_{50}^3, G_{12}^4 and G_{50}^5
- Mass spectra M_η^k models: M_{50}^I, M_{50}^{II}, M_{51}^{III}, M_{35}^I, M_{25}^{II}, M_{15}^{III} and M_{07}^I

For all these models we ran the numerical simulations with 30 000 particles (see § 3.1)

2.3 Observables

2.3.1 Units

Our units are not the commonly used ones (see Heggie & Mathieu (1986)). We did not set the total energy E of the system to -0.25 because we wanted to prescribe instead the initial virial ratio $V_{initial}$, the size R of the system and its mass M. We thus have $M = 1$, $R = 10$ and $G = 1$, and values of $V_{initial}$ and E depending on the simulation. We can link the units

we have used with more standard ones. We have chosen the following relationships between our units of length and mass and common astrophysical ones:

$$M = 10^6 M_\odot \text{ and } R = 10 \ pc \tag{17}$$

Our unit of time u_t is given by:

$$1 u_t = \sqrt{\frac{R_c^3 G_s M_s}{R_s^3 G_c M_c}} \approx 4.72 \ 10^{11} \ s = 1.50 \ 10^4 \ yr \tag{18}$$

where variables X_s are expressed in our simulation units and variables X_c in standard units.

2.3.2   Potential softening and energy conservation

The non conservation of the energy during the numerical evolution has three main sources. The softening parameter ε introduced in the potential calculus (cf. equation 4) is an obvious one. This parameter introduces a lower cutoff Λ in the resolution of length in the simulations. Following Barnes & Hut (1989), structural details up to scale $\Lambda \lesssim 10\varepsilon$ are sensitive to the value of ε. Moreover, in order to be compatible with the collisionless hypothesis, the softening parameter must be greater than the scale where important collisions can occur. Still following Barnes & Hut (1989), this causes

$$\frac{\varepsilon}{10} \gtrsim \frac{G \langle m \rangle}{\langle v^2 \rangle} \tag{19}$$

In our collapse simulation with $3 \cdot 10^4$ particles, this results in $\varepsilon\eta \gtrsim 2/3$. The discretization of time integration introduces inevitably another source of energy non conservation, particularly during the collapse. The force computation also generates errors. The choice of the opening angle Θ, which governs the accuracy of the force calculation of the Treecode, is a compromise between speed and accuracy. For all these reasons, we have adopted $\varepsilon = 0.1$. This choice imposes $\eta \gtrsim 6$ (for $30 \cdot 10^4$ particles). This trade-off allowed to perform simulations with less than 1% energy variation without requiring too much computing time. For each of our experiments, the total CPU time ranges between 3 to 24 hours for 3000 u_t and $3 \cdot 10^4$ particles. The total agregated CPU time of all our collapse experiments is approximately 6 months.

We have tested two other values of the softening parameter ($\varepsilon = 0.03$ and $\varepsilon = 0.3$) for several typical simulations. These tests did not reveal significant variations of the computed observables.

2.3.3 Spatial indicators

As indicators of the geometry of the system, we computed axial ratios, radii containing 10% (R_{10}), 50% (R_{50}) and 90% (R_{90}) of the mass, density profile $\rho(r)$ and equilibrium core radius. The axial ratios are computed with the eigenvalues λ_1, λ_2 and λ_3 of the (3x3) inertia matrix I, where $\lambda_3 \leqslant \lambda_2 \leqslant \lambda_1$ and, if the position of the particle i is $\mathbf{r}_i = (x_{1,i} ; x_{2,i} ; x_{3,i})$

$$
\begin{cases}
I_{\mu\nu} = -\sum_{i=1}^{N} m_i \, x_{\mu,i} \, x_{\nu,i} & \text{for } \mu \neq \nu = 1,2,3 \\[2em]
I_{\mu\mu} = \sum_{i=1}^{N} m_i (r_i^2 - x_{\mu,i}^2) & \text{for } \mu = 1,2,3
\end{cases}
\tag{20}
$$

The axial ratios a_1 and a_2 are given by $a_2 = \lambda_1/\lambda_2 \geqslant 1.0$ and $a_1 = \lambda_3/\lambda_2 \leqslant 1.0$.

The density profile ρ, which depends only on the radius r, together with the R_δ ($\delta = 10, 50, 90$) have a physical meaning only for spherical or nearly spherical systems. For all the spatial indicators computations we have only considered particles whose distance to the center of mass of the system is less than $6 \times R_{50}$ of the system. This assumption excludes particles which are inevitably 'ejected' during the collapse[3].

After the collapse a core-halo structure forms in the system. In order to measure the radius of the core, we have computed the density radius as defined by Casertano and Hut (see Casertano & Hut (1985)). The density radius is a good estimator of the theoretical and observational core radius.

We have also computed the radial density of the system. The density is computed by dividing the system into spherical bins and by calculating the total mass in each bin.

2.3.4 Statistical indicators

When the system has reached an equilibrium state, we compute the temperature of the system

$$
T = \frac{2 \langle K \rangle}{3 N k_B}
\tag{21}
$$

where K is the kinetic energy of the system, k_B is the Boltzmann constant (which is set to 1) and the notation $\langle A \rangle$ denotes the mean value of the observable A, defined by

$$
\langle A \rangle = \frac{1}{N} \sum_{i=1}^{N} A_i
\tag{22}
$$

---

[3] The number of excluded particles ranges from 0% to 30% of the total number of particles, depending mostly on η. For example, the number of excluded particles is 0% for H_{80}, 3% for C_{67}^{20}, 5% for H_{50}, 22% for C_{10}^{20} and 31% for H_{10}.

In order to characterise the system in the velocity space we have computed the function

$$\kappa\left(r\right) = \frac{2\left\langle v_{i,rad}^2 \right\rangle_{r\leqslant r_i<r+dr}}{\left\langle v_{i,tan}^2 \right\rangle_{r\leqslant r_i<r+dr}} \tag{23}$$

where $v_{i,rad}$ is the radial velocity of the i$^{\text{th}}$ particle, and $v_{i,tan}$ its tangential velocity. For spherical and isotropic systems ($a_1 \simeq a_2 \simeq 1$ and $\kappa\left(r\right) \simeq 1$), we have fitted the density by

1- a polytropic law

$$\rho = \rho_0 \psi^{\gamma} \tag{24}$$

which corresponds to a distribution function

$$f\left(E\right) \propto E^{\gamma-3/2} \tag{25}$$

2- an isothermal sphere law

$$\rho = \rho_1 e^{\psi/s^2} \tag{26}$$

which corresponds to a distribution function

$$f\left(E\right) = \frac{\rho_1}{\left(2\pi s^2\right)^{3/2}} e^{\frac{E}{s^2}} \tag{27}$$

Using the least square method in the $\ln(\rho) - \ln(\psi)$ plane we get $(\gamma, \ln\left(\rho_0\right))$ and $(s^2, \ln\left(\rho_1\right))$.

3   DESCRIPTION OF THE RESULTS

We have only studied systems with an initial virial ratio corresponding to $\eta \in [7, 88]$. In such systems, the initial velocity dispersion cannot balance the gravitational field. This produces a collapse. After this collapse, in all our simulations the system reaches an equilibrium state characterised by a temporal mean value of the virial ratio equal to -1, i.e $\eta = 100$, and stationary physical observables. These quantities (defined in section 2) are presented in a table of results in the appendix of this paper. The following results will be discussed and interpreted in section 4.

3.1   Relevant number of particles

In all previous works on this subject (van Albada (1982), Aguilar & Merritt (1990), Cannizzo & Hollister (1992) and Boily et al. (1999)), the authors did not really consider the influence of the number of particles on their results. In the first two and more general works, this number is rather small (not more than a few thousands in the largest simulations). The two other studies are more specific and use typically 10^4 and, in a few reference cases, 2.10^4
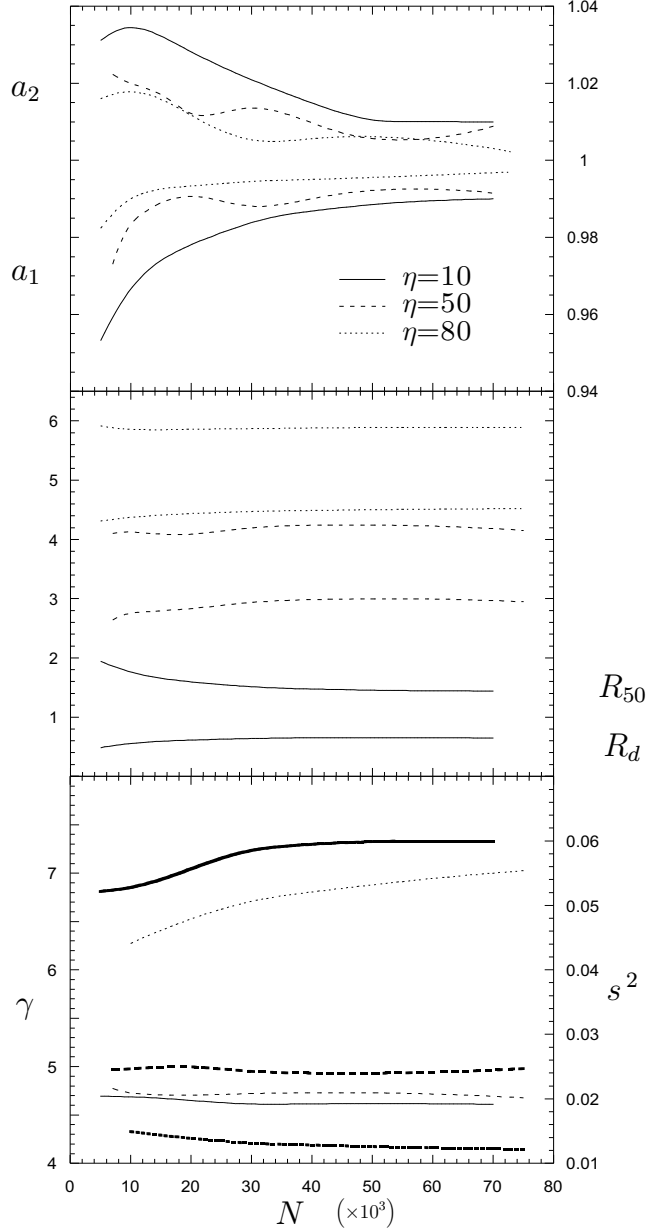
Figure 1. Influence of the number of particles on the physical observables of a collapsing system. Axial ratios are on the top panel, radius containing 50% of the total mass and density radius are on the middle pannel and the best s^2 and γ fit for respectively isothermal and polytropic distribution function are on the bottom panel. All cases are initially homogeneous with $\eta = 10$ (solid line), $\eta = 50$ (dotted line) and $\eta = 80$ (dashed line). The number N of particles used is in units of 10^3.

particles. In order to test the influence of the number of particles on the final results, we have computed several physical observables of some collapsing systems with various numbers of particles. The results are presented in Figure 1. In order to check the influence of N in the whole phase space, we have studied positions and velocities related observables: a_1, a_2, R_{10}, R_{50} and R_{90} and parameters of isothermal and polytropic fit models namely γ and s^2. Moreover, in order to be model-independent, we have studied three representative initial conditions: H_{80}, H_{50} and H_{10}, i.e. respectively initially hot, warm and cold systems. The

number of particles used in each case ranges from 10^2 to 10^5. We can see in Figure 1 that some observables are N-dependent when $N < 3.10^4$. In particular, R_{50} and R_d present a monotonic variation larger than 50% when N varies from 10^2 to 10^5 and the ellipticity of the final state is overestimated for small values of N. As a conclusion of this preliminary study, we claim that the relevant number of particles for collapse simulations is $N \geqslant 3.10^4$. As all simulations have been completed with a total energy loss smaller than 1%, we state moreover that this result is independent of the numerical scheme used (Treecode or Direct N-Body). As a consequence, the simulations presented hereafter have been performed using $N = 3.10^4$ particles.

3.2   Morphological segregation

An important study by Aguilar & Merritt (1990) shows that, in the case of an initial density profile $\rho \propto r^{-1}$, the shape of the virialized state depends on η: a very small η leads to a flattened equilibrium state, when a more quiet collapse produces a spherical one. Our investigations concern a wide range of different initial conditions (homogeneous, clumpy,...) and show that the influence of η depends on the properties of the initial system[4]. Figure 2 shows the axial ratios of the equilibrium state reached by our simulations. In fact, only a few simulations produced a final state with an ellipticity greater than E1. Every homogeneous initial condition (i.e. H_η, G_η^σ and M_η^k) resulted in a spherical equilibrium state independently of the values of η we tested. Cold clumpy systems have a weakly flattened equilibrium state. The only final systems with an ellipticity significantly greater than E1 are those produced by the collapse of cold P_η^α.

Previous studies invoked ROI to explain this morphological segregation. However, it seems that ROI requires inhomogeneities near the center to be triggered.

3.3   Characteristic size segregation

In addition to the morphological segregation, presented in the previous section, we discovered a finer phenomenon.

In the Figures 3, 4, 5, 6 and 7, we have plotted the mass density of all equilibrium states produced by the collapse of our initial conditions as a function of the ratio r/R_{50}. These plots represent the density at the end of our simulations (after about 100 crossing times).

---

[4] The particular case of rotating initial conditions is discussed in a special section.
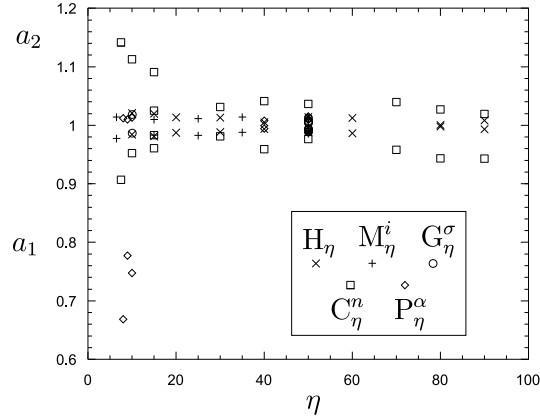
Figure 2. Axial ratios of equilibrium states reached from Homogeneous, Clumpy, Gaussian velocity dispersion, Power law and Mass spectrum initial conditions.
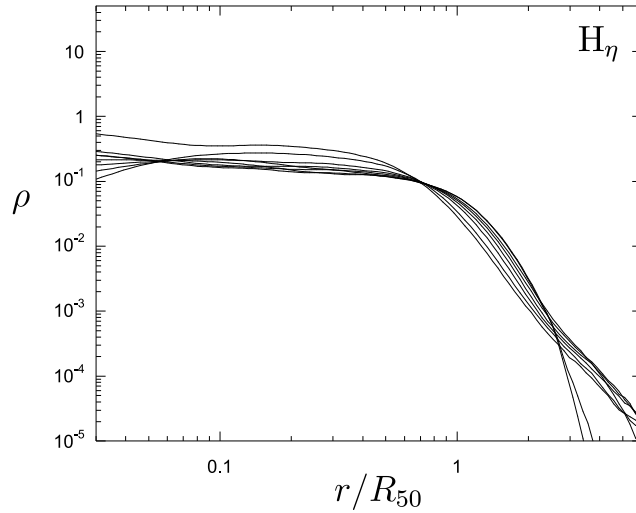
Figure 3. Density profile for H_η models plotted in units of R_{50} .

These functions do not significantly evolve after the collapse except for M_{07}^I. For this special case, a comparative plot is the subject of Figure 8.

All equilibrium states we obtain clearly fall into two categories:

- Flat Core Systems

All these systems present a core halo structure, i.e. a large central region with a constant density and a steep envelope. These systems are typically such that $\ln(R_{50}/R_d) < 0.5$ and $\ln(R_{10}/R_d) < -0.05$.

- Small Core Systems

For such systems, the central density is two order of magnitude larger than for Flat Core
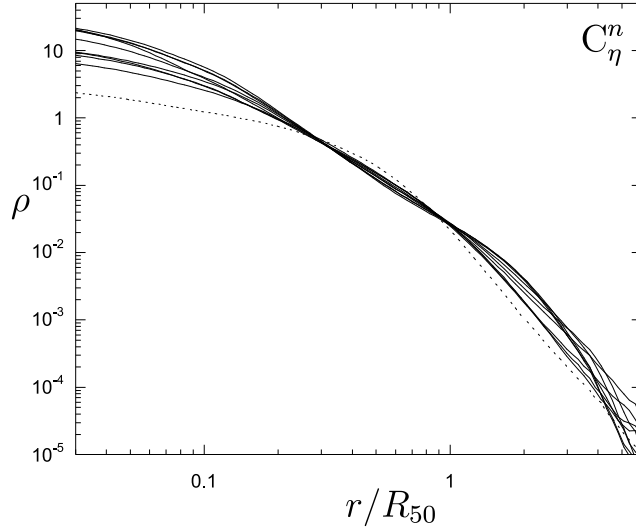
Figure 4. Density profile for C_η^n models plotted in units of R_{50}. The dashed line corresponds to the C_{10}^{03} model
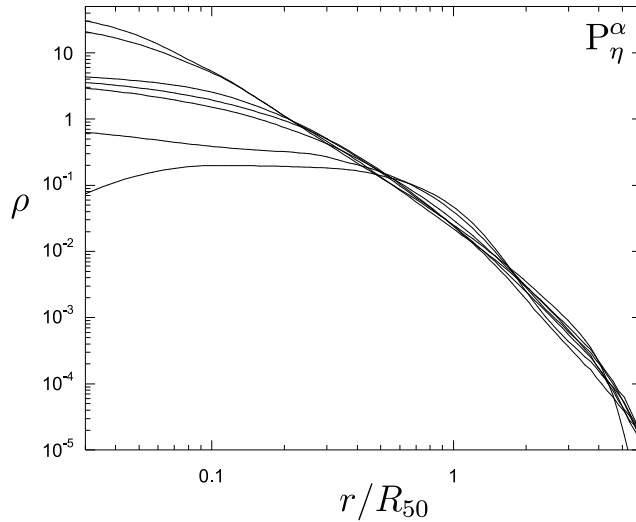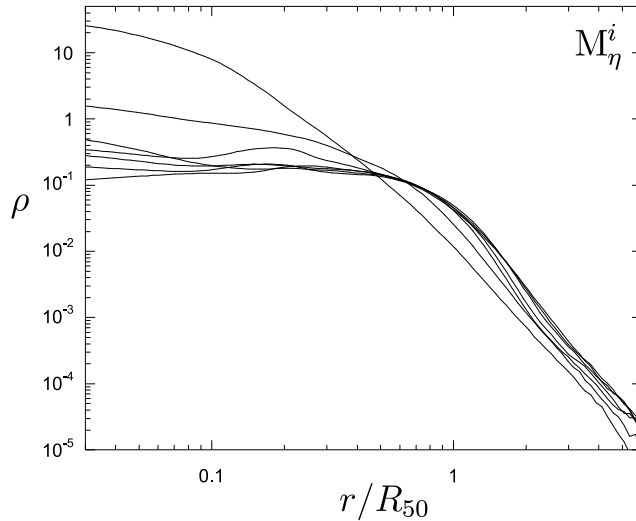

Figure 5. Density profile for P_η^α models plotted in units of R_{50}.

systems. There is no central plateau and the density falls down regularly outward. These systems are typically such that $\ln(R_{50}/R_d) > 0.7$ and $\ln(R_{10}/R_d) > 0.1$.

The diagram $\ln(R_{10}/R_d)$ vs $\ln(R_{50}/R_d)$ is the subject of Figure 9. One can see in this figure that each equilibrium state belongs to one or the other family except in a few particular cases. In the Flat Core family we found all H_η, G_η^σ and M_η^k systems except M_7^I, and two P_η^α systems namely $P_{50}^{0.5}$ and P_{50}^1. These systems are all initially homogeneous or slightly inhomogeneous (e.g. $P_{50}^{0.5}$ and P_{50}^1 systems). In the Small Core family, we found all C_η^{20} and the $P_{50}^{2.0}$ and $P_{09}^{2.0}$ systems. These systems are all initially rather very inhomogeneous. Finally, there are 5 systems in-between the two categories: C_{10}^{03}, $P_{40}^{1.5}$, $P_{08}^{1.5}$, P_{10}^1 and M_{07}^I. This last
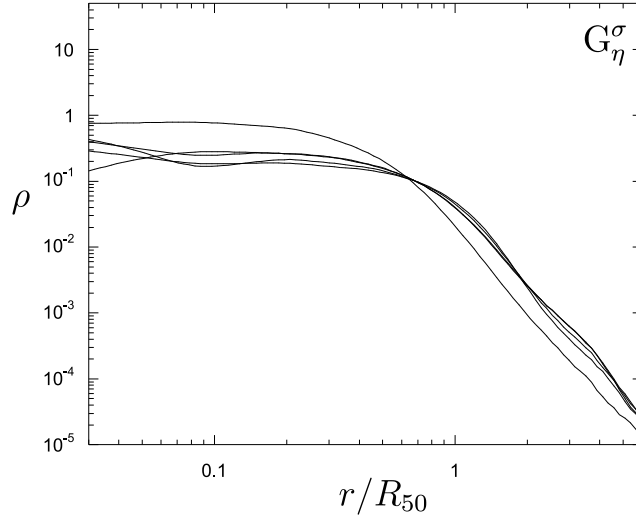
**Figure 6.** Density profile for G_η^σ models plotted in units of R_{50}.

Figure 7. Density profile for M_η^k models plotted in units of R_{50}.

model is the only one which migrates from Flat core set (when $t \simeq 10Td$) to the edge of the small core region (when $t \simeq 100Td$).

3.4 Equilibrium Distribution Function

In order to compare systems in the whole phase space, we fitted the equilibrium state reached by each system with two distinct isotropic models, e.g. polytropic and isothermal (see equations 24-27 or BT87, p.223-232). Figure 10 shows these two fits for the $P_{50}^{0.5}$ simulation. The technique used for the fit is described in section 2 of this paper. The result obtained for this special study is the following: the equilibrium states reached by our initial conditions
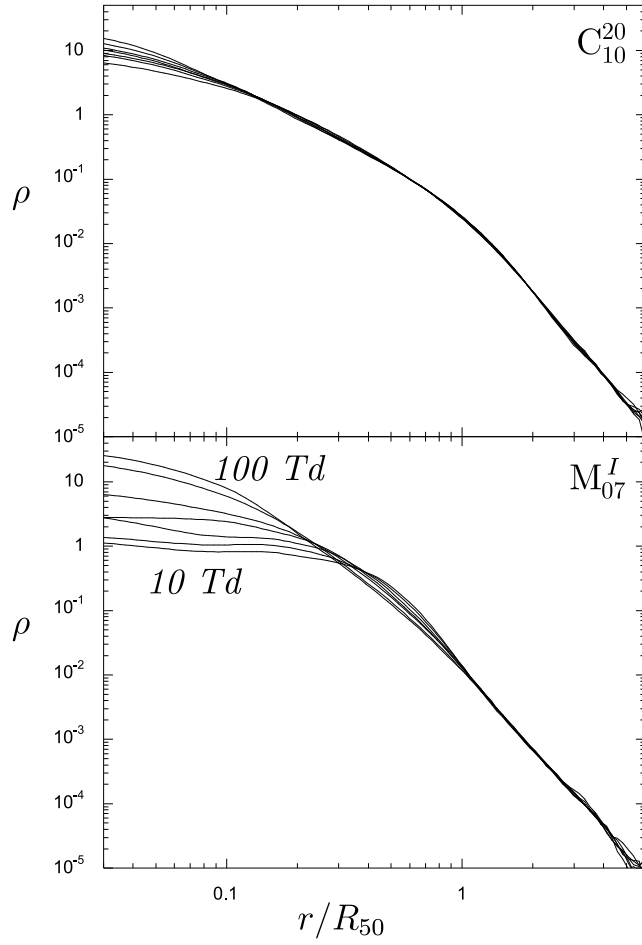
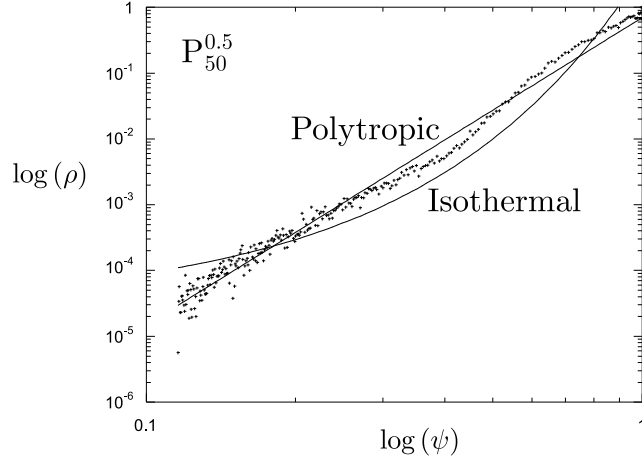**Figure 8.** Comparison between the evolution of the mass density with respect to time for C_{10}^{20} (top-panel) and M_{07}^{I}. For each case, plotted times are 10,20,30,40,50,75 and 100 T_d
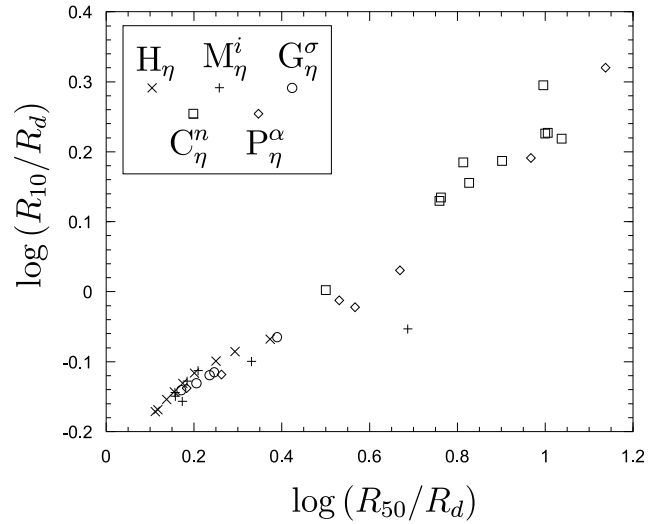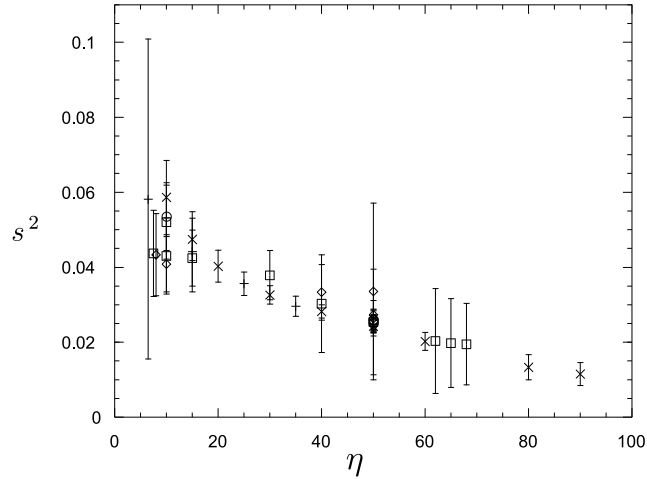

Figure 9. The core size segregation: $\ln(R_{10}/r_c)$ vs $\ln(R_{50}/r_c)$ is plotted for all non rotating systems.

Figure 10. Polytropic and isothermal fit for the $P_{50}^{0.5}$ simulation.

Figure 11. Best fit of the s^2 parameter for an isothermal model for all non rotating systems studied. The error bar correspond to the least square difference between the data and the model.

can be fitted by the two models with a good level of accuracy. As long as $\eta < 70$, the polytropic fit gives a mean value $\gamma = 4.77$ with a standard deviation of $2.48\ 10^{-1}$. This deviation represents 5.1% of the mean value. This value corresponds typically to the well known Plummer model for which $\gamma = 5$ (see BT87 P.224 for details). When the collapse is very quiet (typically $\eta > 70$) polytropic fit is always very good but the value of the index is much larger than Plummer model, e.g. $\gamma = 6.86$ for H_{79} and $\gamma = 7.37$ for H_{88}. The corresponding plot is the subject of the Figure 12. All the data can be found in appendix. As we can see on the example plotted in Figure 10, the isothermal fit is generally not as good as the polytropic one. On the whole set of equilibria, isothermal fits give a mean value $s^2 = 2.5\ 10^{-2}$ with a standard deviation of $1.6\ 10^{-2}$ (60%). The corresponding plot is the subject of Figure 11. All the data can be found in appendix.
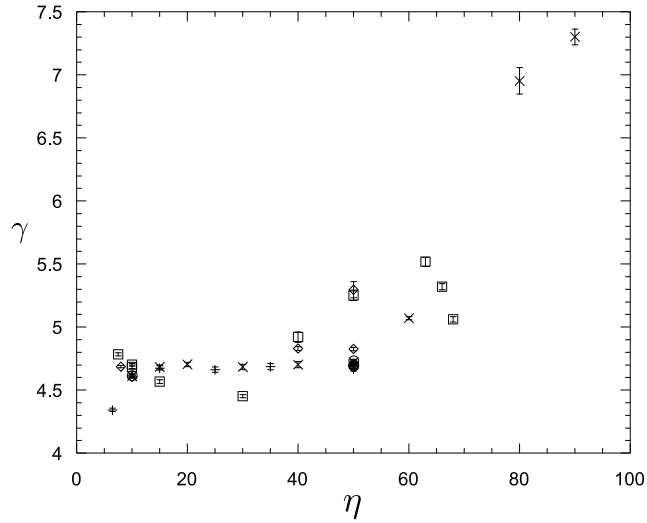
Figure 12. Best fit of the γ parameter for a polytropic model for all non rotating systems studied. The error bars correspond to the least square difference between the data and the model.

In fact both isothermal and polytropic fits are reasonable: as long as the model is able to reproduce a core halo structure the fit is correct. The success of the Plummer model, which density is given by

$$\rho\left(r\right) = \frac{3}{4\pi b^3}\left[1 + \left(\frac{r}{b}\right)^2\right]^{-5/2}$$

can be explained by its ability to fit a wide range of models with various ratio of the core size over the half-mass radius. The adjustment of this ratio is made possible by varying the free parameter b. We expect that other core halo models like King or Hernquist models work as well as the Plummer model. As a conclusion of this section, let us say that as predicted by theory there is not a single universal model to describe the equilibrium state of isotropic spherical self-gravitating system.

3.5   Influence of rotation

We saw in section 3.2 a source of flattening for self-gravitating equilibrium. Let us now show the influence of initial rotation, which is a natural candidate to produce flattening. The way we have added a global rotation and the significance of our rotation parameters f and μ are explained in section 2.2.5. The set of simulations performed for this study contains 31 different elements. The initial virial ratio ranges from $\eta = 10$ to $\eta = 50$, and the rotation parameter from $f = 0$ (i.e. $\mu = 0$) to $f = 20$ (i.e. $\mu = 0.16$ when $\eta = 50$). As a matter of
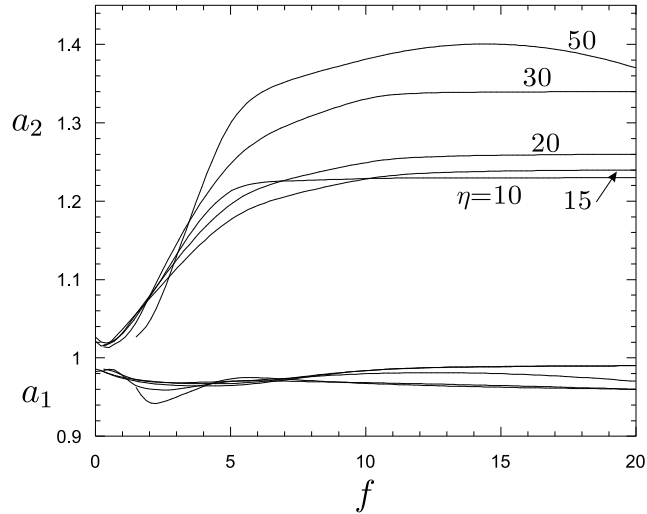
Figure 13. Axial ratios as for different values of η as a function of the initial solid rotation parameter f

fact, equilibrium states always preserve a rather important part of the initial rotation[5] and, observed elliptical gravitating systems generally possess very small amount of rotation (see e.g. Combes et al. (1995)). We thus exclude large values of f .

Our experiments exhibit two main features (see Figure 13): on the one hand, rotation produces a flattened equilibrium state only when f exceeds a triggering value (typically $f = f_o \simeq 4$). On the other hand, we have found that for a given value of η, the flatness of the equilibrium is roughly $f-$independent, provided that $f > f_o$.

3.6 Thermodynamical segregation

As we study isolated systems, the total energy E contained in the system is constant during the considered dynamical evolution . This property remains true as long as we consider collisionless evolutions. For gravitational systems, this means that we cannot carry out any simulation of duration larger than a few hundred dynamical times. We have obviously taken this constraint into account in our experiments. All systems which experience a violent re-laxation reach an equilibrium state which is stationary in the whole phase space. Spatial behaviour like morphological segregation produced by ROI was confirmed and further de-tailled thanks to our study. A new size segregation was found in section 3.3. Now let us consider another new segregation appearing in the velocity space. Each equilibrium state is associated with a constant temperature T, calculated using equation (21). More precisely,

---

[5] We observed that μ is always smaller in the equilibrium state than in the initial one, typically each rotating systems conserves 65% of the initial μ
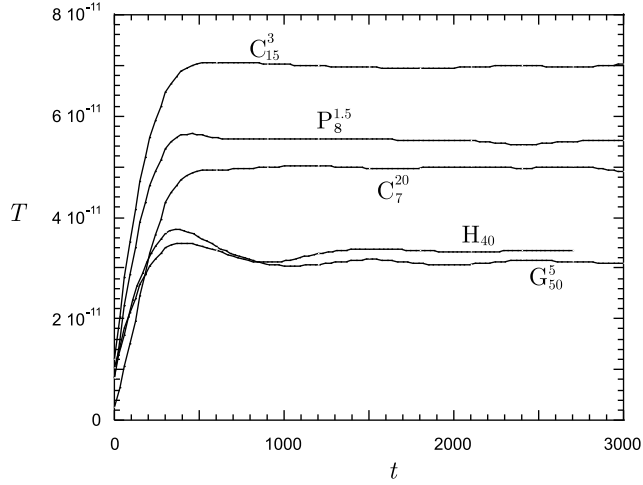
Figure 14. Evolution of the temperature as a function of time
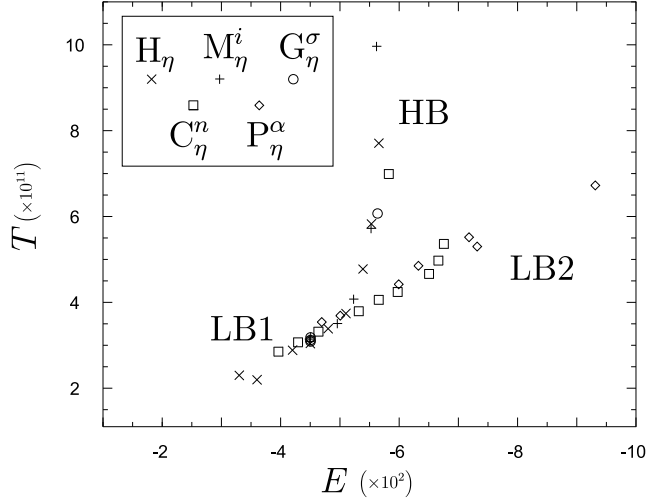
Figure 15. Energy-Temperature diagram

we have calculated the temporal mean value [6] of the temperatures, evaluated every one hundred time units. As we can see in Figure 14, after the collapse and whatever the nature of the initial system is, the temperature is a very stable parameter.

Figure 15 shows the $E - T$ diagram of the set of all non rotating simulations. It reveals a very interesting feature of post-collapse self-gravitating systems.

On the one hand, the set of systems with a total energy $E > -0.054$ can be linearly fitted in the $E - T$ plane. We call this set Low Branch 1 (hereafter denoted by LB1, see Figure 15). On the other hand, the set of the systems with a total energy $E < -0.054$ splits into two families. The first is an exact continuation of LB1. Hence we named it Low Branch 2

---

[6] The temporal mean value is computed from the time when the equilibrium is reached until the end of the simulation

(hereafter denoted by LB2). The second can also be linearly fitted, but with a much greater slope (one order of magnitude). We label this family High Branch (hereafter denoted by HB).

In LB1 or LB2, we find every H, G, and M systems with $\eta > 25$, every P and every C with $n > 10$. In HB, we find C_{10}^{03} and every H, G and M systems with $\eta < 25$. This segregation thus affects violent collapses (cold initial data): on the one hand, when $\eta > 25$ all systems are on LB1, on the other hand for $\eta < 25$, initially homogeneous or quasi-homogeneous (e.g. C_{10}^{03}) systems reach HB when initially inhomogeneous systems stay on LB2 instead.

4   INTERPRETATIONS, CONCLUSIONS AND PERSPECTIVES

Let us now recapitulate the results we have obtained and propose an interpretation:

(i) The equilibrium state produced by the collapse of a set of N gravitating particles is N−independent provided that $N > 3.0\,10^4$.

(ii) Without any rotation, the dissipationless collapse of a set of gravitating particles can produce two relatively distinct equilibrium states:

- If the initial set is homogeneous, the equilibrium has a large core and a steep envelope.
- If the initial set contains significant inhomogeneities ($n > 10$ for clumpy systems or $\alpha > 1$ for power law systems), the equilibrium state has only a small core around of which the density falls down regularly.

The explanation of this core size segregation is clear: it is associated to the Antonov core-collapse instability occurring when the density contrast between central and outward region of a gravitating system is very big. As a matter of fact, if the initial set contains inhomogeneities, these collapse much more quickly than the whole system[7] and fall quickly into the central regions. The density contrast becomes then very large and the Antonov instability triggers producing a core collapse phenomenon. The rest of the system then smoothly collapses around this collapsed core. If there are no inhomogeneities in the initial set, the system collapses as a whole, central density grows slowly without reaching the triggering value of the Antonov instability. A large core then forms. Later evolution can also produce core collapse: this is what occurs for our M_{07}^I system (see Figure 8). This is an initially homogeneous system with Kroupa mass spectrum which suffers a very strong

---

[7] Because their Jeans length is much more smaller than the one of the whole system.

collapse. As the mass spectrum is not sufficient to bring quickly enough a lot of mass in the center of the system, Antonov instability does not trigger and a large core forms. As the collapse is very violent, an increasing significant part of particles are progressively "ejected" and the core collapse takes progressively place. This is the same phenomenon which is generally invoked to explain the collapsed core of some old globular clusters (e.g. Djorgowski et al. (1986)): during its dynamical evolution in the galaxy, some stars are tidally extracted from a globular cluster, to compensate this loss the cluster concentrate its core, increasing then the density contrast, triggering sooner or later the Antonov instability.

(iii) Without any rotation, the collapse (violent or quiet) of an homogeneous set of gravitating particles produces an E0 (i.e. spherical) isotropic equilibrium state. There are two possible ways to obtain a flattened equilibrium:

- Introduce a large amount of inhomogeneity near the center in the initial state, and make a violent collapse ($\eta < 25$).
- Introduce a sufficient amount ($f > 4$) of rotation in the initial state.

These two ways have not the same origin and do not produce the same equilibrium state.

In the first case, one can reasonably invoke the Radial Orbit Instability: as a matter of fact, as it is explained in a lot of works (see Perez et al. (1998) for example) two features are associated to this phenomenon. First of all, it is an instability which needs an equilibrium state from which it grows. Secondly, it triggers only when a sufficient amount of radial orbits are present. The only non rotating flattened systems we observed just combine this two conditions: sufficient amount of radial orbits because the collapse is violent and something from which ROI can grow because we have seen in the previous point that inhomogeneities collapse first and quickly join the center. The fact that cold P_η^α systems are more flattened than C_η^α ones is in complete accordance with our interpretation: as a matter of fact, by construction, power law systems have an initial central overdensity, whereas clumpy systems create (quickly but not instantaneously) this overdensity bringing the collapsed clumps near the center. The ROI flattening is oblate ($a_2 \simeq 1$ and $a_1 < 1$).

The rotational flattening is more natural and occurs when the centrifugal force overcomes the gravitational pressure. The rotational flattening is prolate ($a_2 > 1$ and $a_1 \simeq 1$). We notice that initial rotation must be invoked with parsimony to explain the ellipticity of some globular clusters or elliptical galaxies. As a matter of fact, these objects are very weakly

rotating systems and our study has shown that the amount of rotation is almost constant during the collapse.

(iv) Spherical equilibria can be suitably fitted by both isothermal and polytropic laws with various indexes. It suggests that any distribution function of the energy exhibiting an adaptable core halo structure (Polytrope, Isothermal, King, Hernquist,...) can suitably fit the equilibrium produced by the collapse of our initial conditions.

(v) There exists a temperature segregation between equilibrium states. It concerns only initially cold systems (i.e. systems which will suffer a violent collapse): for such systems when η decreases, the equilibrium temperature T increases much more for initially homogeneous systems than for initially inhomogeneous systems. On the other hand, whatever their initial homogeneity, quiet collapses are rather all equivalent from the point of view of the equilibrium temperature: T increases in the same way for all systems as η decreases. This feature may be the result of the larger influence of the dynamical friction induced by the primordial core on the rapid particles in a violent collapse.

All these properties may be directly confronted to physical data from globular clusters (see Harris catalogue Harris (1996)) or galaxies observations.

As a matter of fact, in the standard "bottom-up" scenario of the hierarchical growth of structures, galaxies naturally form from very inhomogeneous medium. Our study then suggests for the equilibrium state of such objects a potential flattening and a collapsed core. This is in very good accordance with the E0 to E7 observed flatness of elliptical galaxies and may be a good explanation for the presence of massive black hole in the center of galaxies (see Schodel et al. (2002)).

On the other hand Globular Clusters observations show that these are spherical objects (the few low flattened clusters all possess a low amount of rotation), and that their core is generally not collapsed (the collapsed core of almost 10% of the galactic Globular Clusters can be explained by their dynamical evolution through the galaxy). Our study then expect that Globular Clusters form from homogeneous media.

These conclusions can be tested using the $E - T$ plane. As a matter of fact, we expect that an $E - T$ plane build from galactic data would not present any High Branch whereas the same plane build from Globular Clusters data would.

ACKNOWLEDGMENTS

REFERENCES

Aguilar, L., and Merritt, D., 1990, ApJ, 354, 33

Antonov, V.A., Vest. Len. Univ., 7, 135, 1962 in russian translated in english in Dynamics of star clusters, Ed. Goodman J. & Hut P. (IAU 113, Reidel 1985)

Barnes, J. and Hut, P., 1986, Nature, 324, 446

Barnes, J. and Hut, P., 1989, ApJS, 70, 389

Binney, J., and Tremaine, S., 1987, Galactic dynamics, Princeton University Press

Blottiau, P., Bouquet, S., Chièze,J.-P., 1988,A&A, 207, 24

Boily, C.M., Clarke, C.J., Murray, S.D., 1999,M.N.R.A.S., 302, 399

Cannizzo,J.K., and Hollister, T.C., 1992, ApJ, 400, 58

Carpintero,D.D., Muzzio, J.C., 1995, ApJ, 440, 5

Casertano, S., Hut,P., 1985, ApJ, 298, 80

Chavanis, P.-H.,2002,Submitted to Phys. Rev. E, cond-mat/0107345

Chavanis, P.-H., A& A,401, 15, 2003

Combes, F., Boissé, P., Mazure, A., Blanchard, A., 1995, Galaxies and cosmology, Springer Verlag

Dantas, C.C., Capelato, H.V., de Carvalho, R.Ribiero, A.L.B, 2002, A&A, astroph-0201247

Djorgovski, S., King, I. R., Vuosalo, C., Oren, A., Penner, H.,IAU Symp.118, Ed. J.B. Hearnshaw, P.L. Cottrell, 1986

Harris, W.E. 1996, AJ, 112, 1487

Heggie, D.C., and Mathieu R.D., 1986, in The Use of Supercomputers in Stellar Dynamics, ed. P. Hut & S. L. W. McMillan, Springer Verlag.

Hénon, M. , 1960, An.Astro, 23, 472

Henriksen, R.N., and Widrow, L.M., 1995, M.N.R.A.S, 276, 679

Hernquist, 1990, ApJ, 356, 359

Table A1. Homogeneous Initial Conditions: H_η

η	ΔE (%)	η (end)	a_1	a_2	R_{10}	R_{50}	R_{90}	R_d	γ	Σ^2_γ ($\times 10^2$)	s^2 ($\times 10^2$)	$\Sigma^2_{s^2}$ ($\times 10^3$)	T ($\times 10^{11}$)	$-E$ ($\times 10^2$)
88	0.0	98	1.02	0.99	3.39	6.53	10.6	5.02	7.37	-6	1.12	-3	2.30	3.30
79	0.0	99	1.00	1.00	3.11	6.01	9.8	4.59	6.86	-4	1.37	-3	2.20	3.60
60	0.0	96	1.01	0.98	2.41	4.73	11.5	3.41	5.05	-1	2.04	-2	2.89	4.20
50	0.0	96	1.01	0.98	2.04	4.09	15.1	2.81	4.73	-2	2.49	-2	3.04	4.50
40	0.1	96	1.01	0.99	1.72	3.51	25.7	2.30	4.72	-2	2.79	-2	3.39	4.80
30	0.0	96	1.02	0.99	1.36	2.88	253.2	1.75	4.66	-2	3.27	-3	3.74	5.10
20	0.0	101	1.01	0.99	0.95	2.22	874.1	1.17	4.68	-1	4.03	-5	4.78	5.39
15	0.0	108	1.01	0.99	0.74	1.89	1143.0	0.88	4.66	-1	4.73	-6	5.83	5.53
10	1.4	120	1.02	0.98	0.52	1.59	1448.0	0.60	4.59	-1	5.76	-9	7.71	5.66

Table A2. Clumpy Initial Condition: C_η^n

η	n	ΔE (%)	η (end)	a_1	a_2	R_{10}	R_{50}	R_{90}	R_d	γ	Σ^2_γ ($\times 10^2$)	s^2 ($\times 10^2$)	Σ_{s^2} ($\times 10^3$)	T ($\times 10^{11}$)	$-E$ ($\times 10^2$)
10	3	0.1	97	1.03	0.96	0.55	1.85	1241.0	0.58	4.61	-1	5.21	-11	6.99	5.82
67	20	0.8	95	1.01	0.94	0.93	6.14	16.1	0.66	5.00	-1	1.98	-10	2.86	3.96
65	20	0.9	95	1.02	0.96	0.93	5.63	13.5	0.63	5.27	-2	2.00	-13	3.07	4.29
61	20	0.6	95	1.05	0.98	0.86	5.15	12.3	0.58	5.43	-3	2.09	-11	3.32	4.64
48	20	0.6	94	1.03	0.99	0.81	4.24	11.8	0.59	5.15	-3	2.61	-13	3.79	5.31
39	20	0.5	94	1.04	0.99	0.76	3.84	12.8	0.40	4.72	-1	3.20	-10	4.06	5.65
29	20	1.2	94	1.04	0.99	0.72	3.42	15.4	0.56	4.42	-1	3.81	-6	4.24	5.97
14	20	0.3	93	1.09	0.98	0.64	2.72	39.5	0.48	4.56	-1	4.27	-7	4.66	6.50
10	20	1.4	97	1.13	0.99	0.61	2.54	345.5	0.54	4.70	-9	4.25	-15	4.98	6.66
7	20	0.3	94	1.14	0.92	0.57	2.44	224.6	0.45	4.74	-1	4.41	-12	5.36	6.76

Kroupa, P., 2001, M.N.R.A.S., 322, 231

Lancellotti, C.,Kiessling, M., 2001,ApJ, 549, L93

Lynden-Bell, D., and Eggleton, P.P., 1980, M.N.R.A.S., 191, 483

Lynden-Bell, D., 1967, M.N.R.A.S, 136, 601

Nakamura, T.K., 2000, ApJ, 531, 739

Navarro, J.E., White, S.D.M. 1993, M.N.R.A.S., 265, 271

Perez, J. and Aly, J.-J., 1998, M.N.R.A.S., 280, 689

Perez, J. Alimi, J.-M., and Aly, J.-J., 1998, M.N.R.A.S., 280, 700

Salpeter, E.E., 1955, ApJ, 121, 161

R. Schodel, T. Ott, R. Genzel, R. Hofmann, M. Lehnert, A. Eckart, N. Mouawad, T. Alexander, M.J. Reid, R. Lenzen, M. Hartung, F. Lacombe, D. Rouan, E. Gendron, G. Rousset, A.-M. Lagrange, W. Brandner, N. Ageorges, C. Lidman, A.F.M. Moorwood, J. Spyromilio, N. Hubin, K.M. Menten ,17 Oct 2002 ,Nature

Theis, C. and Spurzem, R., 1999, A&A, 341, 361

van Albada, T.S., 1982, M.N.R.A.S., 201, 939

APPENDIX A: TABLES OF RESULTS

Table A3. Power Law Initial Conditions: P_η^α

η	α	ΔE (%)	η (end)	a_1	a_2	R_{10}	R_{50}	R_{90}	R_d	γ	Σ_γ^2 ($\times 10^2$)	s^2 ($\times 10^2$)	Σ_{s^2} ($\times 10^3$)	T ($\times 10^{11}$)	$-E$ ($\times 10^2$)
50	0.5	0.0	95	1.01	0.99	1.84	3.92	13.5	2.53	4.66	-1	2.65	-2	3.54	4.69
50	1	0.0	94	1.01	0.99	1.56	3.77	12.1	2.01	4.77	-6	2.78	-3	3.69	5.00
10	1	0.1	96	1.00	0.80	0.69	2.71	382.2	0.70	4.61	-8	4.05	-8	4.85	6.32
8	1.5	0.1	96	1.01	0.71	0.62	2.63	25.1	0.61	4.63	-7	4.42	-9	5.52	7.18
50	2	1.7	93	1.02	0.99	0.53	3.20	9.2	0.34	5.30	-6	3.35	-9	5.30	7.32
40	1.5	0.1	96	1.00	0.99	0.97	3.31	11.0	1.03	4.71	-8	3.44	-6	4.42	5.99
9	2	1.6	96	1.01	0.78	0.38	2.51	10.6	0.18	4.68	-10	5.21	-20	6.73	9.31

Table A4. Mass Spectrum Initial Conditions: M_η^i

η	i	ΔE (%)	η (end)	a_1	a_2	R_{10}	R_{50}	R_{90}	R_d	γ	Σ_γ^2 ($\times 10^2$)	s^2 ($\times 10^2$)	Σ_{s^2} ($\times 10^3$)	T ($\times 10^{11}$)	$-E$ ($\times 10^2$)
7	Krou	5.0	132	1.02	0.99	0.25	2.04	1721.0	0.37	4.26	-1	5.16	-15	9.97	5.62
15	1/M	0.6	101	1.01	0.98	0.68	2.04	366.8	0.97	4.65	-1	4.35	-10	5.72	5.53
25	Salp	0.4	99	1.01	0.98	1.18	2.51	225.5	1.54	4.66	-2	3.59	-3	4.08	5.23
35	Krou	0.2	98	1.01	0.99	1.55	3.18	39.8	2.09	4.66	-2	2.97	-3	3.51	4.95
51	1/M	0.2	95	1.01	0.98	1.79	4.19	14.2	2.83	4.67	-9	2.39	-4	3.15	4.48
50	Krou	0.1	96	1.02	0.98	1.93	4.09	15.1	2.87	4.60	-1	2.45	-3	3.19	4.50
50	Salp	0.1	96	1.01	0.98	2.03	4.13	15.1	2.87	4.70	-2	2.45	-2	3.08	4.49

Table A5. Gaussian Velocity Dispersion Initial Conditions: G_η^σ

η	σ	ΔE (%)	η (end)	a_1	a_2	R_{10}	R_{50}	R_{90}	R_d	γ	Σ_γ^2 ($\times 10^2$)	s^2 ($\times 10^2$)	$\Sigma_{s^2}^2$ ($\times 10^3$)	T ($\times 10^{11}$)	$-E$ ($\times 10^2$)
48	G1	0.0	95	1.00	1.00	1.72	3.98	14.6	2.23	4.66	-5	2.64	-3	3.13	4.50
49	G2	0.0	95	1.02	0.99	1.74	4.02	14.4	2.28	4.65	-6	2.61	-3	3.13	4.50
50	G3	0.0	95	1.00	1.00	1.90	4.08	14.1	2.56	4.72	-8	2.52	-2	3.09	4.50
12	G4	0.4	118	1.03	0.98	0.56	1.77	1312.0	0.64	4.56	-1	5.33	-10	6.08	5.63
50	G5	0.0	96	1.01	0.99	1.98	4.11	14.8	2.72	4.71	-1	2.50	-2	3.19	4.50